Monthly Notices of the ROYAL ASTRONOMICAL SOCIETY

MNRAS **526,** 4690–4697 (2023) https://doi.org/10.1093/mnras/stad3042
Advance Access publication 2023 October 05

Large-scale turbulence cascade in the spiral galaxy NGC 6946

Meera Nandakumar [1,2]★ and Prasun Dutta[2]★

[1]*Department of Physics, Indian Institute of Science, Bangalore 560012 India*
[2]*Department of Physics, IIT (BHU) Varanasi 221005 India*

Accepted 2023 October 2. Received 2023 August 22; in original form 2023 April 12

ABSTRACT

The generation mechanism of compressible fluid turbulence at kiloparsec scales in the interstellar medium is a long-lasting puzzle. In this work, we explore the nature of large-scale turbulence in the external spiral galaxy NGC 6946. We use the visibility moment estimator to measure the H I column density and line-of-sight turbulent velocity power spectra combining the new observations of A array configuration of Karl G. Jansky Very Large Array (VLA) with the VLA B, C, D array observations from The H I Nearby Galaxy Survey. The estimated power spectra are obeying a power law with a slope of -0.96 ± 0.05 in column density and -1.81 ± 0.07 in line-of-sight velocity in length-scales ranging from 6 kpc to 170 pc. This points towards a forward energy cascade in the plane of the disc with a driving scale at least as large as 6 kpc. The values of the power-law indices indicate a combination of solenoidal and compressive force responsible for driving the measured turbulence. The presence of strong regular magnetic fields from the magnetic spiral arms in the galaxy is possibly contributing to the solenoidal part, while self-gravity or gravitational instability can mostly be the input for the compressive part of the forcing in the driving mechanism.

Key words: turbulence – instrumentation: interferometers – galaxies: ISM – galaxies: kinematics and dynamics – galaxies: structure.

1 INTRODUCTION

Compressible turbulence in the interstellar medium (ISM) plays an important role in governing galactic morphology, dynamics, and chemistry. Compressibility in the turbulent ISM results in the hierarchical formation of scale-invariant structures through which energy cascades in a forward manner from large scales (i.e. few tens of kiloparsec) to smaller scales where star formation is dominant (von Weizsäcker 1951). Through different statistical estimators like probability density function, structure-function, autocorrelation, power spectrum, delta-variance etc., turbulent-generated coherent structures are probed in our Milky Way galaxy at few parsec scales (Crovisier & Dickey 1983; Crovisier, Dickey & Kazes 1985; Green 1993; Deshpande, Dwarakanath & Goss 2000; Dickey et al. 2001; Miville-Deschênes et al. 2003, 2010, 2016; Kauffmann et al. 2010; Roy et al. 2010, 2012; Pingel et al. 2013, 2018; Chepurnov et al. 2015; Marchal & Miville-Deschênes 2021) and in some neighbours like Large Magellanic Clouds (LMCs), Small Magellanic Clouds (SMCs), and other external galaxies at few kpc scales (Stanimirovic et al. 1999; Elmegreen, Kim & Staveley-Smith 2001; Begum, Chengalur & Bhardwaj 2006; Dutta et al. 2008, 2009b; Zhang, Hunter & Elmegreen 2012; Maier et al. 2017; Dib et al. 2021; Pingel et al. 2022). The power spectrum of density and velocity fluctuations coming from the scale-invariant structures obeys a power law in the length-scale region where the energy cascade happens. The possible driving mechanism behind the generation of compressible turbulence in the ISM can be inferred from the power-law indices. For instance, Chepurnov et al. (2010) estimated the velocity statistic of atomic hydrogen emission from Milky Way at high latitudes and interpreted the obtained steep velocity power law at ∼100 pc scales as being due to the shock-dominated turbulence. More similar studies using multiwavelength observations in Milky Way have been conducted and their results along with various simulations suggest that stellar feedback is the possible driver of turbulence at sub-parsec scales (Norman & Ferrara 1996; de Avillez & Breitschwerdt 2004; Mac Low & Klessen 2004; Joung & Mac Low 2006; Hill et al. 2008; Brunt, Heyer & Mac Low 2009; Falceta-Gonçalves, Lazarian & Houde 2010; Ruiz et al. 2013). However, at the larger scales of the order of of kiloparsec, the scenario is different and is still not clearly understood.

Power-spectrum estimation of atomic hydrogen (H I) intensity fluctuations of numerous spiral and dwarf galaxies by Dutta et al. (2013) and Dutta et al. (2009b) shows power-law behaviour at scales ranging from 1 to 10 kpc. The power-law power spectrum obtained in their sample indicates the presence of scale-invariant structures in the ISM, which is attributed to the two-dimensional compressible turbulence. Commonly from the H I intensity distributions, power spectra of column density and line-of-sight turbulent velocity can be estimated, where the latter has information about the driving mechanism of turbulence. Methods like velocity centroids, velocity channel analysis (VCA), and velocity coordinate spectrum (VCS) have been used in literature widely for estimating velocity power spectrum in our Galaxy and dwarf neighbours like SMC and LMC (Lazarian & Pogosyan 2000, 2006; Padoan et al. 2001; Esquivel & Lazarian 2005). However, Dutta (2015) showed that these techniques are not efficient in estimating the velocity power spectrum in

★ E-mail: meeranandakumar93@gmail.com (MN); pdutta.phy@itbhu.ac.in (PD)

external spiral galaxies. Dutta (2016) introduced a method which estimates H I column density and line-of-sight turbulent velocity power spectrum using moments of visibility. Nandakumar & Dutta (2020) implemented a variant of the former, named Visibility Moment power spectrum Estimator (VME), in external spiral galaxy NGC 5236. They measured large-scale turbulence cascades starting from a driving scale of 6 kpc to 300 pc and concluded that it is possibly driven by gravitational instability or self-gravity. Dib & Burkert (2005) showed through autocorrelation length estimation the presence of turbulence cascade with input energy injected at a scale of 6 kpc in dwarf irregular galaxy Holmberg II. Through theoretical modelling, Krumholz & Burkhart (2016) investigated the correlation between star formation rate, gas dispersion, and gas fraction in galaxy models where gravity-driven and feedback-driven turbulence is separately considered. Compared with the observational results on a collection of galaxies, they show that predicted correlations from the gravity-driven model is more agreeing with the observation. In later advanced modelling of disc galaxies, Krumholz et al. (2018) show that for gas-rich high-redshift galaxies, gravity-driven turbulence is required to provide the observed gas dispersion, while in low-redshift galaxies, both feedback and gravity give similar dispersion. In a hydrodynamic simulation of LMC-sized galaxies, Bournaud et al. (2010) show that large-scale turbulence is regulated by gravitational instabilities. Recently Fensch et al. (2023) studied the evolution of gravity-driven isothermal turbulent cascade in disc galaxies and showed that velocity fluctuations obey Burger's scaling. The slope of the velocity power spectrum in their analysis agrees with the estimations of Nandakumar & Dutta (2020) in NGC 5236 within 2 σ uncertainties.

In this paper, we use the VME estimator to measure H I column density and line-of-sight turbulent velocity power spectrum of spiral galaxy NGC 6946. We also compare the earlier results with NGC 5236 and try to make connections between them. NGC 6946 is a bright late-type spiral galaxy. The atomic hydrogen distribution and rotation curve of this galaxy was initially measured by Gordon, Remage & Roberts (1968) using H I observations from a 300 ft radio telescope in National Radio Astronomy Observatory. Later, Tacconi & Young (1986), with the H I observation using Karl G. Jansky Very Large Array (VLA) telescope in the D configuration, detected H I emission in the disc that extends upto a radius of ∼30 kpc. Beck & Hoernes (1996) detected two symmetric bright magnetic spiral arms between the optical spiral arms in NGC 6946 using radio polarization observation. NGC 6946 has well-defined spiral structures and is found to have H I structures like holes and high-velocity gas (Kamphuis & Sancisi 1993; Boomsma et al. 2008). Recently, Khademi & Nasiri (2023) showed that the observed H I gas rotation curve of NGC 6946 is fitted better with a model where the dynamical effect caused by the magnetic fields in the magnetic arms is also taken into account. Dutta et al. (2009b) measured the H I intensity fluctuation power spectrum of NGC 6946 using The H I Nearby Galaxy Survey (THINGS) data. The measured power spectrum has power-law indices of -1.6 ± 0.1 in the range 4 kpc to 300 pc. We present the results of our estimation of H I column density and line-of-sight turbulent velocity power spectrum using VME in NGC 6946. We use the combination of the VLA B, C, and D configuration data from the THINGS survey and new observations taken from the VLA A array configuration in our analysis. The paper is organized as follows: Section 2 discusses the brief overview of the VME estimator, Section 3 describes the observation and further data reduction procedure of NGC 6946. The results of the implementation of VME on calibrated data are presented in Section 4 and inferences on the possible driving mechanism behind the turbulence are discussed in Section 5. We conclude the paper in Section 6 where we present our main findings of this work.

2 BRIEF OVERVIEW ON VISIBILITY MOMENT POWER SPECTRUM ESTIMATOR

Characteristics of a turbulent ISM are imprinted in the two-point correlation functions of its density and velocity fluctuations. These can be probed through observation of H I 21 cm emission using radio interferometers. During the H I 21 cm observations, a radio interferometer measures the visibility function $V(\vec{U}, \nu)$ at the baseline $\vec{U}$ in the observing frequency ν. The baseline is defined as the projected distance between antenna pairs in units of observed wavelengths. For a considerably small portion of the sky, these measured visibilities can be approximated as the Fourier transform of the specific intensity $I(\vec{\theta}, \nu)$ of H I emission coming from any point $\vec{\theta} = (\theta_x, \theta_y)$ in the sky (Thompson, Moran & Swenson 2017). Here, θ_x and θ_y are the Cartesian coordinates in the small patch of the observed sky with the origin at the centre of the field of view of observation. The visibilities are measured only at discrete points sampled by antenna pairs. Since for most of the radio interferometers, the visibilities are not sampled uniformly and regularly in the baseline plane, the observed visibilities provide rather incomplete information about the sky in its Fourier plane. Deconvolution of the sampling pattern is used to generate a specific intensity distribution model of the sky from measured visibilities; however, incomplete baseline coverage of an interferometer makes the deconvolution not an effective tool for estimates of two-point correlations (Dutta & Nandakumar 2019). The two-point correlations can be estimated unbiasedly from the observed visibilities using visibility moment estimator (VME) as follows.

The VME estimates the power spectrum of the H I column density and line-of-sight turbulent velocity of external spiral galaxies using the moments of visibility. Dutta et al. (2009b) estimate the power spectrum of H I intensity fluctuations using visibility correlation estimator and later Dutta & Nandakumar (2019) study the advantage of using this estimator in obtaining unbiased power-spectrum measurement. The VME also uses this method of correlating measurement at the visibility domain for estimating the power spectrum. In a typical interferometric observation though it is expected that visibility correlations are affected by antenna beam pattern, from previous demonstrations of visibility correlation estimator, it is shown that for a galaxy having angular extent of θ_0, these effects can be mitigated at baselines larger than $1/\theta_0$ (Bharadwaj & Sethi 2001; Dutta et al. 2009b). A detailed description of how this is taken care of in VME and their validity tests can be found in Dutta (2016) and Nandakumar & Dutta (2020). We discuss only the basic foundation of these estimators here. The estimators start by taking a zeroth and the first moment of the visibilities with respect to the observing frequencies. The jth moment of the visibility function is defined as $V_j(\vec{U}) = \int \mathrm{d}\nu\, \nu^j\ V(\vec{U}, \nu)$. These moments give information about the column density ($j = 0$) and line-of-sight velocity distributions ($j = 1$). The column density distribution has an imprint on the overall large-scale H I structure of the galaxy as well as the fluctuations due to compressible turbulence. The estimator uses the reconstructed image of the galaxy to estimate the large-scale distribution of H I column density unbiasedly and mitigate its effect from the visibility moment zero ($j = 0$) in the baseline plane to unbiasedly estimate the column density power spectrum. The visibility moment one (i.e. $j = 1$) incorporates the information on column density, the line-of-sight component of the galaxy rotation velocity, and the random turbulent velocity component. The VME uses the estimated column density

Table 1. Table 1 summarizes the various parameters and observational details of NGC 6946: (1) distance to the galaxy, (2) H I inclination angle (i), (3) position angle (p), (4) optical radius (r_{25}), (5) H I major and minor axes, (6) star formation rate, (7) the total H I mass, (8) dynamical mass, and columns (9) to (13) give the details about the new H I observation carried out using VLA telescope. The inclination and position angles given are disc-averaged values and adopted from de Blok et al. (2008). The optical radii r_{25} is the radius where the B-band surface brightness is 25 mag arcsec^{-2} (Walter et al. 2008). The H I extent is defined as the major and minor axis at the level of the column density of 10^{19} atoms cm^{-2} (Dutta et al. 2013).

NGC 6946	
(1) Distance	5.9 Mpc
(2) Inclination angle	33°
(3) Position angle	243°
(4) Optical radius (r_{25})	9.8 kpc
(5) H I extent	35 arcmin × 25 arcmin
(6) Star formation rate	2.52 $M_\odot yr^{-1}$
(7) H I mass	$4.1 \times 10^9 M_\odot$
(8) Dynamical mass	$7.3 \times 10^{11} M_\odot$
(9) VLA observation cycle	VLA 18/A, 19/A
(10) Array Configuration	A (3–170 kλ)
(11) Bandwidth	4 MHz (L band)
(12) Spectral resolution	∼0.4 km s^{-1}
(13) On source time	11 h 36 min

power spectrum from visibility moment zero and the estimates of the galaxy rotation velocity to find the power spectrum of the line-of-sight component of turbulent velocity fluctuations. One of the major assumptions of VME is that the galaxy of interest is a relatively thin face-on disc with an inclination angle in the range ∼15°–40°. NGC 6946 has an average inclination of 33°, well within this requirement.

3 OBSERVATION AND DATA REDUCTION

NGC 6946 is an SABcd-type bright late-type spiral galaxy with prominent spiral structures (de Vaucouleurs et al. 1991; Font et al. 2014). Using the luminosity-based estimate by Karachentsev et al. (2004) we adopt a distance of 5.9 Mpc to the galaxy in our analysis. H I emission from the NGC 6946 has been observed as part of the THINGS survey (Walter et al. 2008). The rotation curve presented in de Blok et al. (2008) shows that the systematic tangential velocity of NGC 6946 is fairly constant for a galactocentric radius greater than 6 kpc. Moreover, the approaching and receding components of the tangential velocity are also quite similar indicating a flatter disc. The dynamical inclination and position angles are found not to vary considerably making it a good choice for the application of VME. The H I line profile width at 20 per cent of the peak intensity for NGC 6946 is 240 km s^{-1}. Table 1 summarizes the various parameters and observational details of NGC 6946. The reasonably larger extent of the H I disc in NGC 6946 helps us to measure the power spectrum to larger length-scales.

As a part of the THINGS survey, NGC 6946 was observed using B, C, and D array configurations of VLA for 10.5, 1.75, and 0.25 h, respectively, with a spectral resolution corresponding to 2.6 km s^{-1}. Using calibrated visibilities from the THINGS survey, Dutta et al. (2013) estimated specific intensity fluctuation power spectra of NGC 6946 by directly using visibility correlations. They found a single power law of slope -1.6 ± 0.1 in length-scale ranging from 300 pc to 4 kpc that fits the H I intensity fluctuation power spectrum. This was considered as an indication of turbulence cascade in the disc. Due to the limited sensitivity and spectral resolution across required ranges of length-scales, THINGS data themselves are not adequate enough for the estimation of the line-of-sight velocity power spectrum. To probe the column density power spectrum to much lower scales as well as to estimate the line-of-sight velocity power spectra we proposed to observe the H I emission from this galaxy with the VLA A array configuration. The intention is to add the information from the VLA A array baseline configurations that have a higher spectral resolution with the already existing baseline coverages from the VLA B C, and D arrays. We observed H I emission from the NGC 6946 using the A array configuration having baseline coverage ranging from 3 to 170 $k\lambda$ at L band in two observation cycles in 2018 and 2019. A total of 14 h of observation was broken down into separate 2 h long observation blocks and carried out in a total of 7 d during the two cycles. In total, we observed the galaxy for a total of 11.6 h in the A array configuration. We use a total bandwidth of 4 MHz (∼845 km s^{-1}) with 2048 channels giving a spectral resolution of ∼0.4 km s^{-1}. The H I emission from our Galaxy contributes within the part of the bandwidth of observation, giving rise to additional emission from the direction of the galaxy and absorption in the spectra of the used bandpass calibrator source. We implemented in-band frequency switching for bandpass calibration and hence accurately spectral calibrated the data. We also identified the channels with extra emissions from our galaxy and flagged them from the observed data. The primary calibration and flagging were carried out in each observational block separately using casa.[1] We combined all the observational blocks into a single data using task 'concat' in casa. Final self-calibration and continuum subtraction procedures were done in this combined data. For continuum subtraction, we make a model of the continuum and subtract it in the uv-space from the visibilities. We use the task 'ft' and 'uvsub' for the continuum subtraction. The calibrated and continuum-subtracted data are then used for further analysis. We also generated a natural weighted clean image cube from the continuum-subtracted visibilities and the required moment maps from this image (see Dutta & Nandakumar 2019 for detail). As mentioned earlier, we include the combined B, C, and D array data from the THINGS survey in our analysis. We received the primary calibrated visibility data from the THINGS survey from Walter et al. (2008) on request. We performed visibility-based continuum subtraction using a similar procedure described here for THINGS data. The final calibrated and continuum-subtracted data from both observations are further used for power-spectrum estimations.

4 RESULTS

Implementation of the VME is discussed in Nandakumar & Dutta (2020). We follow the same procedure here with the calibrated and continuum-subtracted visibilities. We estimate the column density and velocity power spectrum for our new VLA A band observation and the combined B, C, and D array observation from the THINGS survey separately. To calculate the locally averaged intensity moments, we use a two-dimensional Gaussian kernel of width 7 arcmin, which is roughly one-fourth of the H I extent in the disc. Hence, estimated locally averaged intensity moments are used to mitigate the large-scale variation of velocity and density from the estimated visibility correlations as a part of the VME procedure (Dutta & Bharadwaj 2013). The errors of the power spectra are estimated by following the methods used in Dutta (2011).

Using the central 400 channels that correspond to 165 km s^{-1} of the processed visibility data, we estimate the H I column density and

[1]Common Astronomy Software Applications

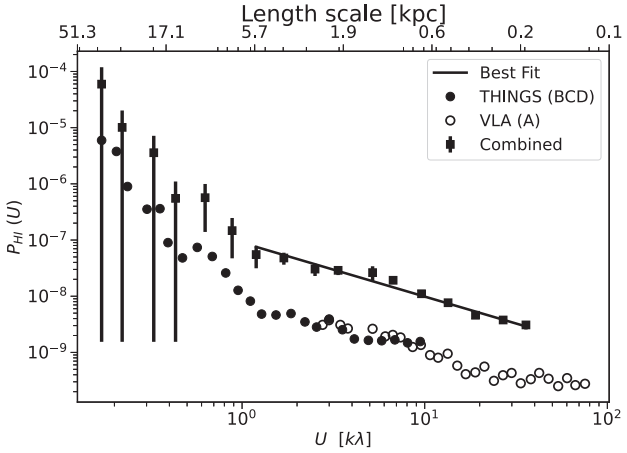

Figure 1. Column density power spectrum of NGC 6946 as a function of baseline U. The corresponding length-scales are also shown in the top margin. The black solid circles correspond to the measurement of the column density from the THINGS data alone. The black open circles correspond to measurement using only the new VLA observations. These two sets of points are scaled down by a factor of 10 for display purposes. The black solid squares with error bars give the power-spectra measurements combining the old THINGS and the new observations. The best-fitting power law to the combined measurement is shown using black solid lines.

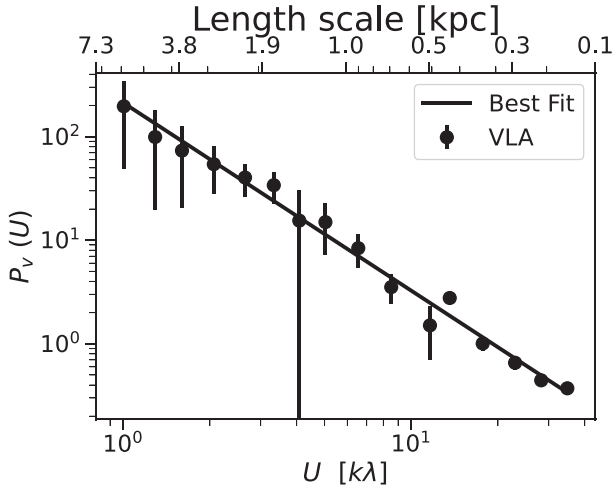

Figure 2. The turbulent velocity power spectrum of NGC 6946 as a function of baseline. The corresponding length-scales are also shown in the top margin. The black solid circles with error bars correspond to the combined measurement. The best-fitting power law to the combined measurement is shown using black solid lines.

Table 2. Result of power-law fit ($P = AU^{\alpha}$) to the column density ($P_{\rm HI}$) and velocity (P_v) power spectra of NGC 6946. The power-law amplitude (A) at one steradian, best-fitting slope α, 1σ errors associated with the fit, the reduced χ^2 values, and the range of fit in baselines and corresponding length-scale ranges are shown. The density power spectra fit is shown for the THINGS data, the new observation data, and the combined power spectra. The amplitudes for the density spectra are scaled by a factor of 10^4 and have a unit of steradian. *The amplitude of the velocity spectra is not scaled and is given in (km s^{-1})^2 steradian.

Data	$P_{\rm HI}(\vec{U})$ THINGS	$P_{\rm HI}(\vec{U})$ New Obs	$P_{\rm HI}(\vec{U})$ Combined	$P_v(\vec{U})$ Combined
$A(\times 10^4)$	0.46 ± 0.08	2.3 ± 0.5	0.67 ± 0.09	59 ± 13*
α	-0.93 ± 0.1	-1.09 ± 0.08	-0.96 ± 0.05	-1.81 ± 0.07
Reduced χ^2	0.7	1.2	1.1	1.2
$U_{\rm min}(k\lambda)$	1	3	1	1
$U_{\rm max}(k\lambda)$	6	36	36	35
$R_{\rm min}(kpc)$	1	0.16	0.16	0.17
$R_{\rm max}(kpc)$	6	2	6	6

line-of-sight velocity power spectrum. Note that we only consider the central part of line emission where the signal-to-noise ratio is much higher. The estimated H I column density power spectrum of different observations is given in Fig. 1. The empty circles show the measurements of the column density power spectrum $P_{\rm HI}$ as a function of baselines using new VLA A array observations and the filled circles show those of THINGS observations. For the THINGS observation also, we use the same part of emission for power spectrum generation. Note that the power spectrum values shown for new VLA and THINGS observations are scaled down by a factor of 10 from their original values for presentation purposes. A power law of $P_{\rm HI} = AU^{\alpha}$ is fitted to these power spectra and fitting parameters are given in Table 2. The column density power spectra estimated from new observation is following a power law from 2 kpc to 160 pc with a slope of -1.09 ± 0.08 and that of THINGS observations has a slope -0.93 ± 0.01 from 6 to 1 kpc. Note that with the new A array observations, we are able to measure the power spectrum up to much smaller length-scales. We merged the estimated power spectra over the entire baseline range and divided them into an equal number of bins on a logarithmic scale. The final combined power spectrum is estimated by taking the average of power spectrum estimates in each logarithmic bin and the respective errors in the bins are calculated by taking the root mean square of the individual error of the estimates in each bin. The black squares with error bars show the combined power spectrum and the black solid line represents the best-fitting power law to the same. Clearly, the combined power spectra also follow a power law in a baseline range of 1–36 kλ, which is equivalent to a length-scale range from 6 kpc to 160 pc in the galactic disc of NGC 6946. The best-fitting values of A and α to the combined power spectra are $(6.7 \pm 0.9) \times 10^{-5}$ steradian and -0.96 ± 0.05. The amplitudes mentioned here are at the baseline of one wavelength. Note that the combined power spectrum (black squares) shows a clear deviation from the power law at smaller baseline of <1 kλ. This is because, at these smaller baselines, the effect from the large-scale features of the disc dominates. The slope of the column density power spectrum of NGC 6946 measured in our analysis matches only at 3σ of uncertainty level with the slope of the intensity fluctuation power spectrum reported by Dutta et al. (2013). Note that the VME of the column density power spectrum suppresses the effect of the window function at lower baselines better than the legacy visibility correlation estimator used earlier. Hence, the slope reported here can be considered more accurate.

Similarly, we estimated the line-of-sight velocity power spectra of THINGS data and new VLA A array observation and combined them to get the final line-of-sight velocity power spectrum. The power spectrum estimates along with the error bars are shown with black circles in Fig. 2. The black solid line represents the best-fitting power law to the estimated power spectrum values. The velocity spectrum obeys a power law of amplitude 59 ± 13 (km s^{-1})^2 steradian and slope -1.81 ± 0.07 in the baseline range 1–35 kλ. This observationally confirms the presence of turbulence cascade in the galactic disc of NGC 6946 in scales ranging from 6 kpc to 170 pc.

Table 3. Power spectral slope for density and velocity for different theoretical models of turbulence, simulations, and observation. Here α is the compressibility factor. ∗Note that though Kolmogorov universal scaling is for incompressible flows, isothermal compressible hydrodynamic simulations for sub/transonic turbulence suggest that the density field also has a similar slope (Kim & Ryu 2005).

Type of turbulence	$P_{\rm HI}(\vec{U})$	$P_v(\vec{U})$	References
Kolmogorov	$-5/3*$	$-5/3$	Kolmogorov (1941)
Burger's	-	-2	Burgers (1948)
Weizsacker	$4\alpha - 2$	$-5/3 - 4\alpha/3$	Fleck (1996)
Solenoidal	-0.78 ± 0.06	-1.86 ± 0.05	Federrath et al. (2009)
Compressive	-1.44 ± 0.23	-1.94 ± 0.05	Federrath et al. (2009)
NGC 5236	-1.23 ± 0.06	-1.91 ± 0.08	Nandakumar & Dutta (2020)
NGC 6946	-0.96 ± 0.05	-1.81 ± 0.07	This work

5 DISCUSSION

Our measurement of column density and line-of-sight turbulent velocity power spectrum of H I in spiral galaxy NGC 6946 indicates the presence of a large-scale energy cascade in the disc. In the power spectra of dust emission in LMC and nearby galaxy M33 and that of H I emission of NGC 1058, a break in the spectra has been observed at the scales nearer to the scale height of the galaxy (Dutta et al. 2009a; Block et al. 2010; Combes 2012). Dutta et al. (2009b) have demonstrated using numerical simulation that a 2D–3D transition gives rise to a change in the slope of the power spectrum. They find the relation between the angular scale in which the change in slope happens and the scale height of the disc depends on the disc profile. Körtgen, Pingel & Killerby-Smith (2021) also reported that the scale at which the power-law index changes is not the scale height of the disc but related to it. The scale at which the break is observed is larger than the scale height of the disc (see Dutta et al. 2009b). This broken power law is interpreted as a transition from large-scale two-dimensional structures to small- scale three-dimensional structures at the scale height of the disc. Koch et al. (2020) show that the change in a slope is also observed at an angular scale related to the PSF of the telescope. This effect is particular to the power-spectrum estimation from images due to the existence of pixels smaller than the telescope resolution (Dutta & Nandakumar 2019). Interestingly, in our measurement, we do not see any transition or break in the power law in both column density and velocity power spectra in the entire range where the cascading is happening. Hence the power-law power spectra of both density and velocity can be interpreted as the two-dimensional structure that is generated by turbulence in the disc.

The slope of the power-law power spectra of column density and line-of-sight turbulent velocity is the quantifier that tells us about the nature of the turbulence. For instance, in incompressible fluid turbulence, Kolmogorov theory predicts that the slope of the velocity power spectra is $-\frac{5}{3}$ (Kolmogorov 1941). In the case of compressible fluid, though a well-established theory is not yet introduced, several analytically computational models are proposed (Burgers 1948; von Weizsäcker 1951; Fleck 1996). The expected slope of the power spectra proposed in these models is given in Table 3. Federrath, Klessen & Schmidt (2009) find the slope of column density and velocity power spectra of compressible fluid turbulence driven by different types of forcing using numerical simulations. The slope of H I column density and turbulent velocity power spectra of NGC 5236 indicate that the driving force that generates turbulence therein is compressive in nature (Nandakumar & Dutta 2020). For the galaxy NGC 6946, the density power spectrum has a slope of -0.96. Using the scaling relation between density and velocity power-spectrum slope for compressible fluid turbulence by Fleck (1996), the velocity power spectrum slope for NGC 6946 is expected to be -2.01. This is consistent with our measured slope of -1.80 ± 0.13 within 2σ uncertainties. The slope of the velocity fluctuation power spectra for two different forcing mechanisms, solenoidal and compressive, is rather similar in the Federrath et al. (2009) analysis and it is difficult to use the measured slope of the velocity fluctuation power spectrum only to comment on the nature of turbulence forcing. However, the density fluctuation assumes different power-law slopes for different forcing mechanisms, making the slope of the density fluctuation power spectrum an indicator of the forcing mechanism. The column density slope of -0.96 is intermediate to the slopes found for compressive and solenoidal forcing by Federrath et al. (2009). We believe that the turbulence-driving mechanism for NGC 6946 comes from a combination of compressive and solenoidal forcing. The following subsection discusses the various possible drivers that can be attributed to the measured turbulence.

5.1 Nature of turbulence in NGC 6946

Comparing the slopes of our power spectra estimations with the various theoretical and simulation models of turbulence in the literature, we find that the input energy to the turbulence in NGC 6946 likely comes partly from solenoidal and partly from compressive forcing. The compressive forcing can arise from the self-gravity of the gas on large scales like in the case of NGC 5236 found by Nandakumar & Dutta (2020). The findings by Romeo & Fathi (2015) and Romeo & Mogotsi (2017) that the disc instability process triggers fragmentation in molecular gas essentially support our results. The known sources for solenoidal forcing in the galactic discs are the differential rotation which generates shear and additional influence of magnetic field in the disc (Sellwood & Balbus 1999; Federrath et al. 2010). Large-scale galactic magnetic fields are observed in several external spiral galaxies using radio synchrotron emission (Chyży & Buta 2008; Krause 2009; Beck 2013). The typical field strength observed in spiral arms is 1–10 μG (Sofue, Fujimoto & Wielebinski 1986). Inter-arm magnetic fields, known as magnetic arms, are also observed. Such magnetic arms are found to be present in NGC 6946 (Beck et al. 1996). Beck (2007) reports multiple strong magnetic spiral arms (having field strength of ∼20 μG) in NGC 6946 using radio polarization observation. On their investigation of magnetic properties in this galaxy, the measured total magnetic energy density is found to be of a similar order in the inner part of the galactic disc (<2 kpc) compared to the outer part (up to 10 kpc). The ordered magnetic fields are found to be present in NGC 6946 up to a radius of ∼12 kpc and regular magnetic fields are detected up to ∼15 kpc in Beck (2007) observations. These detected ordered fields are aligned along with the spiral structures which indicates the possible interaction of the gas in the arms with a magnetic field.

Applying a non-linear turbulent dynamo model to the NGC 6946, through numerical studies, Rohde, Beck & Elstner (1999) show that observed magnetic structures in NGC 6946 can be well reproduced. These results suggest the observed magnetic structures are the result of turbulent dynamics in the disc. Hence we are here to conclude that the magnetic field of NGC 6946 may have a major role to drive its large-scale turbulence.

The power-law behaviour in the power spectra shows an energy cascade in an inertial range starting from 6 kpc to 170 pc. For the measured power-law slope of −0.96 for column density fluctuations, the expected slope of the corresponding autocorrelation function is 1.04. At scales of 6 kpc, these correspond to a standard deviation in column density fluctuations of 0.01. For NGC 5236, the inertial range begins at scales of 11 kpc, where the standard deviation in column density fluctuation estimated is 0.011 at those scales (Nandakumar & Dutta 2020). By scaling the estimated standard deviations of density fluctuations compared with the latter, the standard deviation in column density fluctuations at 11 kpc for NGC 6946 is twice that of NGC 5236.

Though the velocity of gas has three vector components v_x, v_y, and v_z in its galactic coordinates, in a real observation what measures is the line-of-sight velocity $v_{\rm los}$. v_x and v_y are the velocity components along the plane of the disc and v_z is the vertical velocity component. For a typical galaxy, having an inclination angle i, the line-of-sight component is given as $v_{\rm los} = -v_y \sin i + v_z \cos i$. Hence the autocorrelation function of the line-of-sight velocity, $\xi_{\rm los}$, in terms of different velocity components is

$$\begin{aligned}\xi_{\rm los}(|\vec{\theta}' - \vec{\theta}|) &= \langle v_{\rm los}(\vec{\theta}) v_{\rm los}(\vec{\theta}')\rangle \\ &= \xi_y \sin^2 i + \xi_z \cos^2 i, \end{aligned} \quad (1)$$

where the autocorrelation function of the vertical component v_z is $\xi_z(|\vec{\theta}' - \vec{\theta}|) = \langle v_z(\vec{\theta}) v_z(\vec{\theta}')\rangle$ and that of the planar component v_y is $\xi_y(|\vec{\theta}' - \vec{\theta}|) = \langle v_y(\vec{\theta}) v_y(\vec{\theta}')\rangle$. Note that here we assumed that any cross-correlation terms between the on-plane and off-the-plane motions are negligible. Bournaud et al. (2010) estimate the power spectrum of the different components of velocity fields from a hydrodynamic galaxy simulation. They show the power spectra of on-plane and vertical components of velocity in length-scales from ∼1.5 kpc to ∼10 pc, where all three components follow the same power law at smaller scales. At larger scales of the order of kiloparsecs, on-plane components follow the same power law; however, the perpendicular component flattens at larger scales greater than the disc thickness. This is expected in thin-disc galaxies, where the large amplitude of the motion of gas happens in the galactic plane. A similar trend of flattening has been found in the power spectrum of the vertical component at similar scales in the numerical simulation studies on gravity-driven turbulence cascade in the disc by Fensch et al. (2023). Hence we can infer the turbulent velocity fluctuations in the plane of the disc as follows from equation (1) after assuming that the right term in the equation is negligible. In our estimations, we see that the line-of-sight turbulent velocity fluctuation power spectrum of NGC 6946 has a power law with a slope of −1.81. This corresponds to a slope of 0.19 to the autocorrelation function of the line-of-sight velocity $\xi_{\rm los}$ and hence the standard deviation of 27.1 km s^{-1} in turbulent velocity fluctuations at 6 kpc scales in the plane of the disc.

The energy input rate per unit area by the ISM turbulence can be estimated using $\epsilon \sim \frac{1}{2} \times (N_{\rm H_{I_0}} m_{\rm H_I}) \times (v^T)^2 \times v^T / L$, where $N_{\rm H_{I_0}}$ is the average column density over the disc, $m_{\rm H_I}$ is the mass of atomic hydrogen, and v^T is the turbulent velocity fluctuation. The quantity $N_{\rm H_{I_0}} m_{\rm H_I}$ gives the mass of H I in turbulence per unit area, and L/v^T gives the time-scale of energy input. We find from the moment zero map of NGC 6946 the value of $N_{\rm H_{I_0}}$ as 3.7×10^{20} atoms cm^{-2}. Considering the energy input scale is at 6 kpc, we find the turbulence energy input $\sim 3 \times 10^{-7}$ ergs cm^{-2} s^{-1}. For NGC 5236, this corresponds to an energy input of $\sim 1.4 \times 10^{-7}$ ergs cm^{-2} s^{-1} at similar scales. An average rate of a supernova that happens once in 100 yr and releases around 10^{51} erg (Mackey et al. 2017) of kinetic energy would give an energy input rate per unit area of $\sim 1 \times 10^{-6}$ ergs cm^{-2} s^{-1} in the H I disc of NGC 6946 after considering an efficiency factor of $\epsilon_{SN} \sim 0.1$ to convert the ejected kinetic energy to turbulent motions (Thornton et al. 1998; Tamburro et al. 2009). Note that the energy input from the supernovae is around six times of the measured turbulent energy at 6 kpc scales. However, whether the kinetic energy input from supernovae can reach such large scales coherently is still questionable.

6 CONCLUSION

It is well established now that the large-scale turbulence cascade is present in the ISM of disc galaxies. Though in small scales it is well clear from both observation and simulations that the stellar feedback is enough to supply energy consistently to the cascade in molecular cloud scales; whether the same is enough to drive the turbulence in the galactic scale where diffuse atomic gas is prominently seen is still in debate. Numerous observational studies on external galaxies support the stellar feedback in sustaining the energy required for large-scale cascades (Bacchini et al. 2020). Utomo, Blitz & Falgarone (2019) conduct multiwavelength studies of M33 to investigate the origin of ISM turbulence therein, where they did the comparison of calculated turbulent energy with energy input from various sources like supernovae, magneto-rotational instability, and gravitational instability. Their results strongly suggest that upto to a galactic radius of 7 kpc, supernovae alone are enough to maintain the observed turbulent energy, while the contribution from others is not sufficient. Contradicting to it, Koch et al. (2018) showed in the same galaxy that both the energy inputs from supernovae and MRI cannot explain the observed turbulent energy input. Various other numerical simulations on turbulent ISM also suggest that stellar feedback is not enough to sustain the turbulence at kiloparsec scales (Bournaud et al. 2010; Krumholz & Burkhart 2016). Modelling a star-forming ISM that has self-consistent stellar feedback, Colman et al. (2022) estimate the power spectrum of coherent density structures where they see that when the turbulence is driven only by stellar feedback, the power spectrum flattens at scales of 60 pc which is roughly the average length-scale of the supernova feedback. Fensch et al. (2023) introduce numerical simulation on isothermal turbulent cascade in disc galaxy which is purely driven by gravity and estimates power spectra of gas velocity and density. The slope of the velocity power spectra in their estimates obeys Burger's scaling (∼−2 see Table 3), similar to our estimates found on both NGC 6946 and NGC 5236. Agreement with former results suggests that the compressive component of the driving force to the measured cascade is contributed by gravity. One of the possible factors that contribute to the solenoidal part of the driving mechanism is the large-scale ordered magnetic field indirectly coupling with the gas and hence generating an energy cascade. Federrath et al. (2017) probed the turbulence in Galactic region G0.253+0.016 and suggest that shear causes the turbulence. Hence another possibility here that generates solenoidal turbulence is the galactic shear generated by the differential rotation in the disc. In the lack of sufficient observational results, numerical simulations of the turbulent disc with different types of driving forces should be conducted and compared in order to establish the contribution

of various galactic phenomena in creating the energy cascade in the disc.

In this work, we present evidence of the gas turbulence cascade in galactic scales in disc galaxy NGC 6946. We use the VME to measure the H I column density and line-of-sight turbulent velocity power spectrum from VLA observations. Comparing our results from the earlier estimations on NGC 5236, we see that irrespective of the similar inertial range of cascade, the generating mechanism that drives turbulences is different in the two galaxies. To understand the universal picture of the turbulence generation in the ISM of galaxies, measurement of the turbulence cascade at galactic disc on a large number of galaxies and interpreting hence the obtained results with various numerical simulations is required. We would like to proceed in this direction in future.

ACKNOWLEDGEMENTS

We thank Nirupam Roy for his helpful suggestions during the observations with VLA. MN acknowledges the Department of Science and Technology – Innovation in Science Pursuit for Inspired Research (DST-INSPIRE) fellowship for funding this work. PD acknowledges DST-INSPIRE faculty fellowship support for this work. MN acknowledges the postdoctoral fellowship support from Max-Planck-Gesellschaft Partner Group Grant and support from the Indian Institute of Science, Bangalore. We thank the staff of the NRAO that made these observations possible. The National Radio Astronomy Observatory is a facility of the National Science Foundation operated under a cooperative agreement by Associated Universities, Inc. We thank the anonymous referee for suggestions that have improved the presentation of the paper significantly.

DATA AVAILABILITY

The uncalibrated raw visibility data of VLA A array observation of NGC 6946 are publicly available on NRAO Data Archive website (https://data.nrao.edu). The final calibrated visibility data used in this paper will be shared on reasonable request to the corresponding author.

REFERENCES

Bacchini C., Fraternali F., Iorio G., Pezzulli G., Marasco A., Nipoti C., 2020, A&A, 641, A70
Beck R., 2007, A&A, 470, 539
Beck R., 2013, Springer, New York, in Beck R., Balogh A., Bykov A., Treumann R. A., Widrow L.eds,, Vol. 39, Large-Scale Magnetic Fields in the Universe. Series: Space Sciences Series of ISSI. p. 215
Beck R., Brandenburg A., Moss D., Shukurov A., Sokoloff D., 1996, ARA&A, 34, 155
Beck R., Hoernes P., 1996, Nature, 379, 47
Begum A., Chengalur J. N., Bhardwaj S., 2006, MNRAS, 372, L33
Bharadwaj S., Sethi S. K., 2001, J. Astrophys. Astron., 22, 293
Block D. L., Puerari I., Elmegreen B. G., Bournaud F., 2010, ApJ, 718, L1
Boomsma R., Oosterloo T. A., Fraternali F., van der Hulst J. M., Sancisi R., 2008, A&A, 490, 555
Bournaud F., Elmegreen B. G., Teyssier R., Block D. L., Puerari I., 2010, MNRAS, 409, 1088
Brunt C. M., Heyer M. H., Mac Low M. M., 2009, A&A, 504, 883
Burgers J., 1948, Elsevier, Von Mises R., Von Karman T., Advances in Applied Mechanics,1, p.171
Chepurnov A., Burkhart B., Lazarian A., Stanimirovic S., 2015, ApJ, 810, 33
Chepurnov A., Lazarian A., Stanimirović S., Heiles C., Peek J. E. G., 2010, ApJ, 714, 1398
Chyży K. T., Buta R. J., 2008, ApJ, 677, L17
Colman T. et al., 2022, MNRAS, 514, 3670
Combes F. e. a., 2012, A&A, 539, A67
Crovisier J., Dickey J. M., 1983, A&A, 122, 282
Crovisier J., Dickey J. M., Kazes I., 1985, A&A, 146, 223
de Avillez M., Breitschwerdt D., 2004, Ap&SS, 289, 479
de Blok W. J. G., Walter F., Brinks E., Trachternach C., Oh S.-H., Kennicutt R. C., Jr, 2008, AJ, 136, 2648
de Vaucouleurs G., de Vaucouleurs A., Corwin Herold G. J., Buta R. J., Paturel G., Fouque P., 1991, Springer,New York,Third Reference Catalogue of Bright Galaxies
Deshpande A. A., Dwarakanath K. S., Goss W. M., 2000, ApJ, 543, 227
Dib S. ,Braine J.,Gopinathan M.,Lara-López M. A.,Kravtsov V. V.,Soam A.,Sharma E.,Zhukovska S.,Aouad C.,Belinchón J. Antonio,Helou G.,Li D. (2021) A&A,655 ,A101, p.20
Dib S., Burkert A., 2005, ApJ, 630, 238
Dickey J. M., McClure-Griffiths N. M., Stanimirović S., Gaensler B. M., Green A. J., 2001, ApJ, 561, 264
Dutta P., 2011, preprint (arXiv:1102.4419)
Dutta P., 2015, MNRAS, 452, 803
Dutta P., 2016, MNRAS, 456, L117
Dutta P., Begum A., Bharadwaj S., Chengalur J. N., 2008, MNRAS, 384, L34
Dutta P., Begum A., Bharadwaj S., Chengalur J. N., 2009a, MNRAS, 397, L60
Dutta P., Begum A., Bharadwaj S., Chengalur J. N., 2009b, MNRAS, 398, 887
Dutta P., Begum A., Bharadwaj S., Chengalur J. N., 2013, New Astron., 19, 89
Dutta P., Bharadwaj S., 2013, MNRAS, 436, L49
Dutta P., Nandakumar M., 2019, Res. Astron. Astrophys., 19, 060
Elmegreen B. G., Kim S., Staveley-Smith L., 2001, ApJ, 548, 749
Esquivel A., Lazarian A., 2005, ApJ, 631, 320
Falceta-Gonçalves D., Lazarian A., Houde M., 2010, ApJ, 713, 1376
Federrath C. et al., 2017, in Crocker R. M., Longmore S. N., Bicknell G. V.eds, Proc. IAU Symp. 322, The Multi-Messenger Astrophysics of the Galactic Centre. Kluwer, Dordrecht, p. 123
Federrath C., Klessen R. S., Schmidt W., 2009, ApJ, 692, 364
Federrath C., Roman-Duval J., Klessen R. S., Schmidt W., Mac Low M. M., 2010, A&A, 512, A81
Fensch J., Bournaud F., Brucy N., Dubois Y., Hennebelle P., Rosdahl J., 2023, A&A, 672, A193
Fleck Robert C. J., 1996, ApJ, 458, 739
Font J., Beckman J. E., Zaragoza-Cardiel J., Fathi K., Epinat B., Amram P., 2014, MNRAS, 444, L85
Gordon K. J., Remage N. H., Roberts M. S., 1968, ApJ, 154, 845
Green D. A., 1993, MNRAS, 262, 327
Hill A. S., Benjamin R. A., Kowal G., Reynolds R. J., Haffner L. M., Lazarian A., 2008, ApJ, 686, 363
Joung M. K. R., Mac Low M.-M., 2006, ApJ, 653, 1266
Kamphuis J., Sancisi R., 1993, A&A, 273, L31
Karachentsev I. D., Karachentseva V. E., Huchtmeier W. K., Makarov D. I., 2004, AJ, 127, 2031
Kauffmann J., Pillai T., Shetty R., Myers P. C., Goodman A. A., 2010, ApJ, 716, 433
Khademi M., Nasiri S., 2023, ApJ, 945, 36
Kim J., Ryu D., 2005, ApJ, 630, L45
Koch E. W. et al., 2018, MNRAS, 479, 2505
Koch E. W., Chiang I.-D., Utomo D., Chastenet J., Leroy A. K., Rosolowsky E. W., Sandstrom K. M., 2020, MNRAS, 492, 2663
Kolmogorov A., 1941, Akademiia Nauk SSSR Doklady, 30, 301
Körtgen B., Pingel N., Killerby-Smith N., 2021, MNRAS, 505, 1972
Krause M., 2009, Magnetic Fields in the Universe II (2008),Esquivel A., in J. Franco,G. García-Segura,E. M. de Gouveia Dal Pino,A. Lazarian & A. Raga,Revista Mexicana de Astronomia y Astrofisica (SC),36, p.25
Krumholz M. R., Burkhart B., 2016, MNRAS, 458, 1671
Krumholz M. R., Burkhart B., Forbes J. C., Crocker R. M., 2018, MNRAS, 477, 2716
Lazarian A., Pogosyan D., 2000, ApJ, 537, 720
Lazarian A., Pogosyan D., 2006, ApJ, 652, 1348

Mac Low M.-M., Klessen R. S., 2004, Rev. Mod. Phys., 76, 125
Mackey A. D., Koposov S. E., Da Costa G. S., Belokurov V., Erkal D., Fraternali F., McClure-Griffiths N. M., Fraser M., 2017, MNRAS, 472, 2975
Maier E., Elmegreen B. G., Hunter D. A., Chien L.-H., Hollyday G., Simpson C. E., 2017, AJ, 153, 163
Marchal A., Miville-Deschênes M.-A., 2021, ApJ, 908, 186
Miville-Deschênes M. A. et al., 2010, A&A, 518, L104
Miville-Deschênes M. A., Duc P. A., Marleau F., Cuillandre J. C., Didelon P., Gwyn S., Karabal E., 2016, A&A, 593, A4
Miville-Deschênes M. A., Joncas G., Falgarone E., Boulanger F., 2003, A&A, 411, 109
Nandakumar M., Dutta P., 2020, MNRAS, 496, 1803
Norman C. A., Ferrara A., 1996, ApJ, 467, 280
Padoan P., Kim S., Goodman A., Staveley-Smith L., 2001, ApJ, 555, L33
Pingel N. M. et al., 2013, ApJ, 779, 36
Pingel N. M. et al., 2022, Publ. Astron. Soc. Aust., 39, e005
Pingel N. M., Lee M.-Y., Burkhart B., Stanimirović S., 2018, ApJ, 856, 136
Rohde R., Beck R., Elstner D., 1999, A&A, 350, 423
Romeo A B.,Fathi Kambiz,2015,MNRAS, 451,3107
Romeo A.B,Mogotsi K.M.,2017,MNRAS, 469 ,286
Roy N., Chengalur J. N., Dutta P., Bharadwaj S., 2010, MNRAS, 404, L45
Roy N., Minter A. H., Goss W. M., Brogan C. L., Dutta P., Chengalur J. N., Lazio T. J. W., 2012, in American Astronomical Society Meeting Abstracts #219. p. 320.05
Ruiz L. O., Falceta-Gonçalves D., Lanfranchi G. A., Caproni A., 2013, MNRAS, 429, 1437
Sellwood J. A., Balbus S. A., 1999, ApJ, 511, 660
Sofue Y., Fujimoto M., Wielebinski R., 1986, ARA&A, 24, 459
Stanimirovic S., Staveley-Smith L., Dickey J. M., Sault R. J., Snowden S. L., 1999, MNRAS, 302, 417
Tacconi L. J., Young J. S., 1986, ApJ, 308, 600
Tamburro D., Rix H.-W., Leroy A. K., Mac Low M.-M., Walter F., Kennicutt R. C., Brinks E., de Blok W. J. G., 2009, AJ, 137, 4424
Thompson A. R., Moran J. M., Swenson George W. J., 2017, Springer,Interferometry and Synthesis in Radio Astronomy, 3rd Edition
Thornton K., Gaudlitz M., Janka H. T., Steinmetz M., 1998, ApJ, 500, 95
Utomo D., Blitz L., Falgarone E., 2019, ApJ, 871, 17
von Weizsäcker C. F., 1951, ApJ, 114, 165
Walter F., Brinks E., de Blok W. J. G., Bigiel F., Kennicutt Robert C. J., Thornley M. D., Leroy A., 2008, AJ, 136, 2563
Zhang H.-X., Hunter D. A., Elmegreen B. G., 2012, ApJ, 754, 29

This paper has been typeset from a TEX/LATEX file prepared by the author.